The Astrophysical Journal, 908:129 (7pp), 2021 February 20 https://doi.org/10.3847/1538-4357/abd1d5
© 2021. The American Astronomical Society. All rights reserved.

Discovery of a Damped Lyα Galaxy at $z \sim 3$ toward the Quasar SDSS J011852+040644

Ravi Joshi[1], Michele Fumagalli[2,3,4], Raghunathan Srianand[5], Pasquier Noterdaeme[6], Patrick Petitjean[6], Marc Rafelski[7,8], Ruari Mackenzie[4,9], Qiong Li[1,10], Zheng Cai[11], D. Christopher Martin[12], Siwei Zou[1], Xue-Bing Wu[1,10], Linhua Jiang[1], and Luis C. Ho[1,10]

[1] Kavli Institute for Astronomy and Astrophysics, Peking University, Beijing 100871, People's Republic of China; rvjoshirv@gmail.com
[2] Dipartimento di Fisica G. Occhialini, Università degli Studi di Milano Bicocca, Piazza della Scienza 3, I-20126 Milano, Italy
[3] Institute for Computational Cosmology, Durham University, South Road, Durham, DH1 3LE, UK
[4] Centre for Extragalactic Astronomy, Durham University, South Road, Durham, DH1 3LE, UK
[5] Inter-University Centre for Astronomy and Astrophysics, Post Bag 4, Ganeshkhind, Pune 411007, India
[6] Sorbonne Université, CNRS, UMR 7095, Institut d'Astrophysique de Paris, 98 bis bd Arago, F-75014 Paris, France
[7] Space Telescope Science Institute, Baltimore, MD 21218, USA
[8] Department of Physics & Astronomy, Johns Hopkins University, Baltimore, MD 21218, USA
[9] Department of Physics, ETH Zurich, Wolfgang-Pauli-Strasse 27, 8093 Zurich, Switzerland
[10] Department of Astronomy, School of Physics, Peking University, Beijing 100871, People's Republic of China
[11] Department of Astronomy, Tsinghua University, Beijing 100084, People's Republic of China
[12] Cahill Center for Astrophysics, California Institute of Technology, 1216 East California Boulevard, Mail Code 278-17, Pasadena, CA 91125, USA
Received 2019 September 4; revised 2020 November 10; accepted 2020 December 4; published 2021 February 18

Abstract

We report the detection of the host galaxy of a damped Lyα system (DLA) with $\log N(\mathrm{H\,I})\,[\mathrm{cm}^{-2}] = 21.0 \pm 0.10$ at $z \approx 3.0091$ toward the background quasar SDSS J011852+040644 using the Palomar Cosmic Web Imager at the Hale (P200) telescope. We detect Lyα emission in the dark core of the DLA trough at a 3.3σ confidence level, with Lyα luminosity of $L_{\mathrm{Ly}\alpha} = (3.8 \pm 0.8) \times 10^{42}\,\mathrm{erg\,s^{-1}}$, corresponding to a star formation rate of $\gtrsim 2\,M_{\odot}\,\mathrm{yr}^{-1}$ (considering a lower limit on Lyα escape fraction $f_{\mathrm{esc}}^{\mathrm{Ly}\alpha} \sim 2\%$) as typical for Lyman break galaxies at these redshifts. The Lyα emission is blueshifted with respect to the systemic redshift derived from metal absorption lines by $281 \pm 43\,\mathrm{km\,s^{-1}}$. The associated galaxy is at very small impact parameter of $\lesssim 12$ kpc from the background quasar, which is in line with the observed anticorrelation between column density and impact parameter in spectroscopic searches tracing the large-scale environments of DLA host galaxies.

Unified Astronomy Thesaurus concepts: Quasar absorption line spectroscopy (1317); Damped Lyman-alpha systems (349); Star formation (1569)

1. Introduction

The evolution of galaxies is significantly influenced by the physical state of gas in and around the central star-forming regions. Observations of local galaxies indicate that the atomic and molecular hydrogen, which make up most of the mass in the interstellar medium of galaxies, closely trace the star formation rate and are the key elements that participate in inflows and outflows (Bigiel et al. 2008; Genzel et al. 2010; Cortese et al. 2011; Janowiecki et al. 2017).

Unfortunately, mapping neutral hydrogen (H I) gas in emission from galaxies is difficult at even moderate redshifts (Kanekar et al. 2016). This low density gas imprints, however, absorption lines on the spectra of an unrelated bright background source, which offers a powerful tool to study the physical and chemical properties of the intervening gas in a luminosity independent manner (see Wolfe et al. 2005, for a review). At high redshift, most of our knowledge of H I gas primarily comes from a particular class of absorption line systems, the damped Lyα absorbers (DLAs) seen in quasar spectra. With an H I column density of $\geqslant 2 \times 10^{20}\,\mathrm{cm}^{-2}$, DLAs account for the bulk (>80%) of the neutral hydrogen in the early universe (Péroux et al. 2003; Noterdaeme et al. 2009, 2012; Prochaska & Wolfe 2009).

Moreover, DLAs appear to be linked to star-forming regions, as evidenced by the metallicity evolution of DLAs with redshift (Rafelski et al. 2012, 2014; Jorgenson et al. 2013) and the velocity spread of low-ion absorption lines (see Wolfe et al. 2005). The average properties of Lyα emission from DLAs, inferred from the stacking experiment of hundreds of DLAs from the Sloan Digital Sky Survey (SDSS), further indicate a connection between star formation activity and outflows in DLA host galaxies (see also, Rahmani et al. 2010; Noterdaeme et al. 2014; Joshi et al. 2017). Therefore, establishing a direct association of the H I gas seen in absorption with emission from galaxies is a useful way to probe the link between the H I gas and star formation at high redshift.

Earlier efforts to detect DLA host galaxies either in continuum emission or nebular line emission have been moderately successful in completely blind surveys, with a detection rate of ∼10% (Möller et al. 2004), with several studies mostly resulting in non-detections (Kulkarni et al. 2000; Christensen et al. 2009; Fumagalli et al. 2015). Leveraging the observed correlation between luminosity and metallicity in galaxies (Tremonti et al. 2004; Ledoux et al. 2006; Møller et al. 2013; Christensen et al. 2014), recent campaigns have focused instead on metal-rich DLAs, resulting in a far higher detection rate of ≈65% (Fynbo et al. 2010, 2011; Krogager et al. 2017; Ranjan et al. 2020).

In spite of these numerous attempts, however, only ≈20 DLAs at redshift $\gtrsim 2$ have been associated directly with counterparts in emission (see Krogager et al. 2017). This low detection rate could be attributed either to the faint nature of DLA galaxies (which become difficult to image at close separation from bright background quasars), or to their dusty nature, or to high H I column density, or yet again to the fact that only a fraction of the DLA population is directly connected to active star formation.

More recently, interferometers such as the Atacama Large Millimeter/submillimeter Array (ALMA) have overcome the

dust bias, with the detection of ∼10 molecular gas-rich systems using CO rotational transitions and the atomic [C II] line (Neeleman et al. 2016, 2018; Fynbo et al. 2018; Klitsch et al. 2019). So far, these studies have focused on tracing relatively high-metallicity systems, finding the DLA hosts at relatively large impact parameters, ∼16–45 kpc, and with high molecular gas masses of 10^{10}–$10^{11} M_{\odot}$. Following these successes, efforts to detect more representative DLAs are ongoing.

Furthermore, the use of integral field spectrographs (IFSs) at 8–10 m class telescopes has proven to be a very efficient tool for searching DLA galaxies and for characterizing their environment out to several hundreds of kiloparsecs (Péroux et al. 2011, 2012; Fumagalli et al. 2017; Mackenzie et al. 2019). For example, using the MUSE IFS at the Very Large Telescope (VLT) telescope, Fumagalli et al. (2017) have detected a tantalizing example of extended Lyα emission tracing gas in a region of about 50 kpc near a $z \approx 3$ DLA. This region hosts multiple galaxies, possibly in a filament, with Lyα emission induced by in situ star formation likely triggered by interactions.

Moreover, in a recent MUSE survey of 6 DLAs at $z \sim 3$, Mackenzie et al. (2019) have obtained a high detection rate of galaxies up to ≈80% within 1000 km s^{-1} of the DLAs, with impact parameters ranging between 25 and 280 kpc. Notably, in contrast to previous searches, the blind survey of Mackenzie et al. (2019) has yielded detections of multiple galaxies also for low metallicity systems (see their Figure 9), including a galaxy group associated with a metal-poor DLA ($Z/Z_{\odot} \approx -2.33$). With a small but representative sample, using cosmological simulations, these authors have been able to place constraints on the typical mass of halos that host DLAs in the range 10^{11}–$10^{12} M_{\odot}$.

To further understand the link between H I gas and star formation near the peak of the cosmic star formation activity, we have started a survey to search for high-redshift ($z \gtrsim 3$) DLA host galaxy counterparts in Lyα emission using the Palomar Cosmic Web Imager (PCWI). In this article, we present results from a pilot observation that traces the large-scale environment of a strong intervening DLA with $\log N(\mathrm{H\,I})[\mathrm{cm}^{-2}] = 21.0 \pm 0.10$ at $z_{\rm abs} \approx 3.0091$ out to 80 kpc. Our observations lead to the discovery of the host galaxy, revealing a direct association of the absorbing gas with star formation, with no other counterpart within the field of view $20'' \times 40''$. This paper is organized as follows. Section 2 describes the sample selection. In Section 3, we present the observations and data reduction. In Section 4, we present results of our analysis, followed by a discussion and conclusion in Section 5. Throughout, we have assumed a flat universe with $H_0 = 70$ km s^{-1} Mpc^{-1}, $\Omega_{\rm m} = 0.3$ and $\Omega_{\Lambda} = 0.7$.

2. Sample Selection

Using the compilation of thousands of DLAs from SDSS (Noterdaeme et al. 2012), we have selected a subset having high H I column density, with $\log N(\mathrm{H\,I})\ [\mathrm{cm}^{-2}] \geqslant 21$, which provides the favorable environment for star formation and thus is likely to trace regions in close proximity to star-forming galaxies (Krogager et al. 2012; Altay & Theuns 2013). Moreover, at these high column densities, the Lyα absorption has a dark (optically thick) core, which spreads over at least seven times the average full-width at half-maximum (FWHM, ≈160 km s^{-1}) of the instrumental profile of the SDSS spectrograph. This makes it possible to search for Lyα emission lines within the spectrum.

We consider only the DLAs detected in SDSS spectra with a median continuum-to-noise ratio > 3 which ensure an accurate determination of the H I column density. In addition, we avoid DLAs that are proximate to the quasars by considering only systems with velocity offsets of >5000 km s^{-1} with respect to the quasar emission redshift. We also exclude sightlines showing broad absorption lines from quasar outflows. To avoid introducing a metallicity bias, we do not preselect targets based on metal lines (e.g., Si II, Fe II, C II).

In order to maximize the detection rate of Lyα emission, we further search the spectra to identify systems with tentative Lyα emission (non-zero flux) within the absorption trough where the quasar continuum goes to zero (i.e., the dark core). For this, we avoid the regions with bright sky emission to exclude the false positives due to residuals of the sky subtraction. Due to the finite fiber size of SDSS, this step introduces a selection effect, that is, detections are expected to primarily occur at small impact parameters of $\lesssim$15 kpc (see below). An example of a system selected in this way, which is also the target of our pilot observations, is shown in the upper panel of Figure 1.

Following visual inspection to remove systems with clear sky residuals or artifacts, this selection resulted in a unique set of 13 DLAs (out of 608) with absorption redshifts $z \geqslant 2.9$. Among them, 10 systems lie at declinations that Hale (P200) can reach and are suitable for P200 observations. As a further verification of the presence of possible Lyα emission, we have also examined the multi-epoch observations from SDSS, which exists for three DLAs in our sample. Reassuringly, all three systems show Lyα emission in spectra at different epochs, albeit with low signal-to-noise ratio (S/N). In order to be able to detect the minimum Lyα emission flux of $\sim 2 \times 10^{-17}$ erg s^{-1} cm^{-2} found in our sample, an integration of ∼1 hr on source and ∼1 hr on sky would allow us to detect the emission feature at more than $\sim 5\sigma$ level. In what follows, we present the results for the first target successfully observed so far.

3. Observations and Data Reduction

We have performed observations of the quasar SDSS J011852 +040644 ($z_{\rm em} \approx 3.226$) with an intervening DLA system from our selection above ($z_{\rm abs} \approx 3.0091$ and $\log N(\mathrm{H\,I})\ [\mathrm{cm}^{-2}] = 21.0 \pm 0.1$) using the PCWI instrument mounted on the Hale 5 meter telescope on Mt. Palomar. PCWI uses a $40'' \times 60''$ reflective image slicer with 24 slices of dimension $40'' \times 2\farcs5$ each. The observations have been conducted on the night UT 20180816 with a clear sky and with airmass ranging between 1 and 2. We have used the Richardson (MedRez) gratings with a slit-limited spectral resolution of $\Delta\lambda \sim 1$ Å.

The individual exposures were acquired using the standard PCWI nod-and-shuffle technique, where the central 1/3 of the CCD is used for recording the spectrum while masking the outer 2/3 of the CCD, restricting the spectral bandpass to ∼150 Å (see Martin et al. 2014). Note that our DLA sample is preselected based on the likely presence of Lyα emission within the $2''$ or $3''$ SDSS-III or SDSS-II fiber spectra. Thus, it is expected that the DLA host galaxy lies at small impact parameters (i.e., ∼8–12 kpc). However, to trace the large-scale environment around the quasar, while performing nod-and-shuffle, we offset the frame by $25''$ so that the quasar remains within the frame at all times. We acquired a series of 1200 s exposures, totaling 1.6 hr with the quasar at the center, and 1.6 hr after the offset. Combined, this technique doubles the total integration time for the object, to 3.3 hr. This strategy

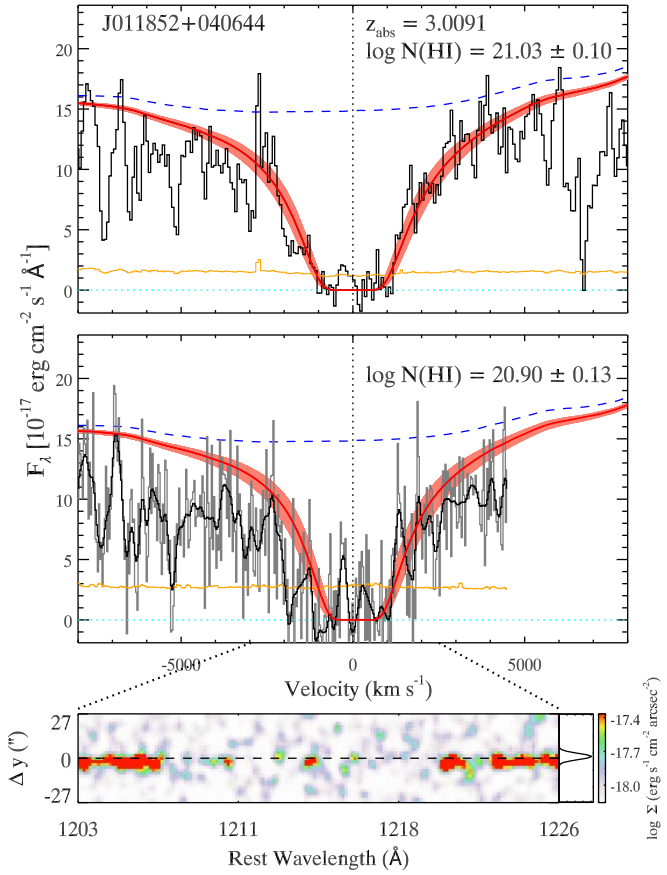

Figure 1. Top panel: the Lyα absorption profile in the SDSS spectrum (black histogram) in the velocity scale with respect to $z_{abs} \sim 3.0091$. The estimated unabsorbed quasar continuum is shown as a blue dashed curve along with the error spectrum using the dotted–dashed curve. The continuum template modified by the damped Lyα absorption is shown with a red solid line, marking the profile uncertainty corresponding to 1σ error in column density with a red shaded region. Middle panel: 1D quasar spectrum from the original PCWI data (gray histogram) and following resampling at the SDSS resolution of 2.5 Å (black histogram). A new model fit derived on PCWI data, which is consistent with the SDSS estimate, is also shown. Bottom panel: 2D quasar spectrum constructed from PCWI data cube. The trace of the quasar is shown as a dashed line.

resulted in an effective field of view of $20'' \times 40''$ with the quasar at the center which allowed us to search for the DLA host galaxy and trace its large-scale environment out to $\approx$80 kpc ($\approx 10''$ at $z \sim 3$).

The data are reduced with the standard PCWI pipeline (Martin et al. 2014). The flux calibration was performed using the standard star BD+28D4211, observed on the same night, and the final data cube is combined by weighting individual exposures according to their inverse variance. In addition, the wavelengths are converted into their values in vacuum. The final cube has a pixel size of $\sim 1\farcs5$ in the spatial direction, and 0.55 Å in the wavelength direction. In addition, the spatial resolution of PCWI cube is appearing limited along the slices in the short direction, which at the time of observations was $1\farcs4$, and slit limited ($\sim 2\farcs5$) in the long direction.

4. Results

With the final PCWI data cube in hand, we first extract the quasar spectrum in an aperture with radius of $3''$, which is twice the FWHM and encompasses the total quasar emission. In

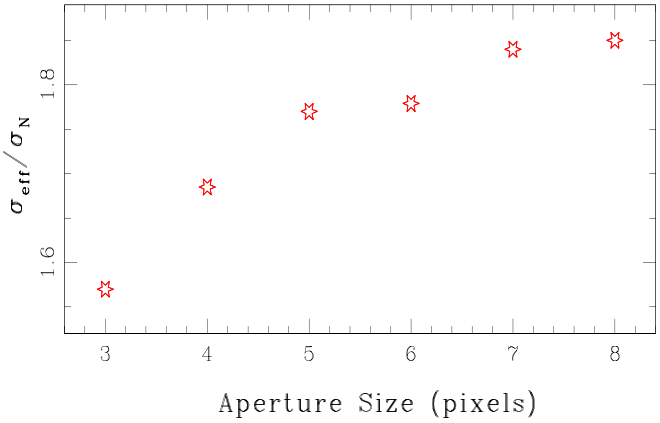

Figure 2. Ratio between the flux dispersion in apertures of varying size (σ_{eff}) and the error computed propagating the pixel standard deviation (σ_N), which is useful to assess the impact of correlated noise within the PCWI data cube.

Figure 1, we compare the DLA absorption profile in the flux-calibrated 1D quasar spectrum from our moderate-resolution ($R \sim 5000$) PCWI data (middle panel) with the lower-resolution ($R \sim 2000$) SDSS fiber spectrum (top panel). The best fit continuum is shown with a dashed (blue) curve, which is modeled with a quasar composite template from Harris et al. (2016) by adjusting the continuum power-law slope and normalization to fit the quasar continuum over the Lyα forest. It is clear that the DLA absorption profile and quasar continuum level agree well in both spectra. Next, we measure the H I column densities by fitting Voigt profiles to the Lyα lines in the flux-calibrated SDSS and PCWI spectra, as shown in Figure 1. The modeled absorption profile touches the unabsorbed region of the spectrum, but also due to the low resolution, there are regions that are absorbed by the forest. The derived N(H I) from the lower-resolution SDSS spectrum is $\log N(\mathrm{H\,I})[\mathrm{cm}^{-2}] = 21.03 \pm 0.10$, while our PCWI data result in $\log N(\mathrm{H\,I})[\mathrm{cm}^{-2}] = 20.90 \pm 0.13$. Both measurements are consistent with each other and with the measurement of $\log N(\mathrm{H\,I})[\mathrm{cm}^{-2}] = 21.0 \pm 0.10$ presented in Noterdaeme et al. (2012).

In line with the preselection from SDSS, we clearly see an emission line signature in the DLA core at the expected position based on the SDSS spectrum. This is also evident from the reconstructed 2D spectrum from the PCWI data cube (see lower panel of Figure 1). To quantify the detection significance of the Lyα emission, we first need to account for any correlated noise introduced by the resampling of individual pixels in the final data cube. Such correlated noise typically results in an underestimate of the effective noise inside an aperture and thus in an overestimate of the real S/N of a source (Gawiser et al. 2006; Fumagalli et al. 2014).

To model the noise variation as a function of aperture size, we compute the effective noise $\sigma_{\rm eff}$ as the standard deviation of fluxes by considering only the regions free from the continuum detected sources across the PCWI data cube over cubic apertures of four spectral pixels ($\sim$4 Å) and a variable aperture size in the spatial direction. Figure 2 shows the ratio between this effective noise ($\sigma_{\rm eff}$) and the error computed by propagating the variance (σ_N) as a function of apertures size. Ratios above unity indicate that the pipeline noise is underestimated by a factor of $\sim$50% for an aperture of $\sim 3''$. We account for this effect throughout our analysis.

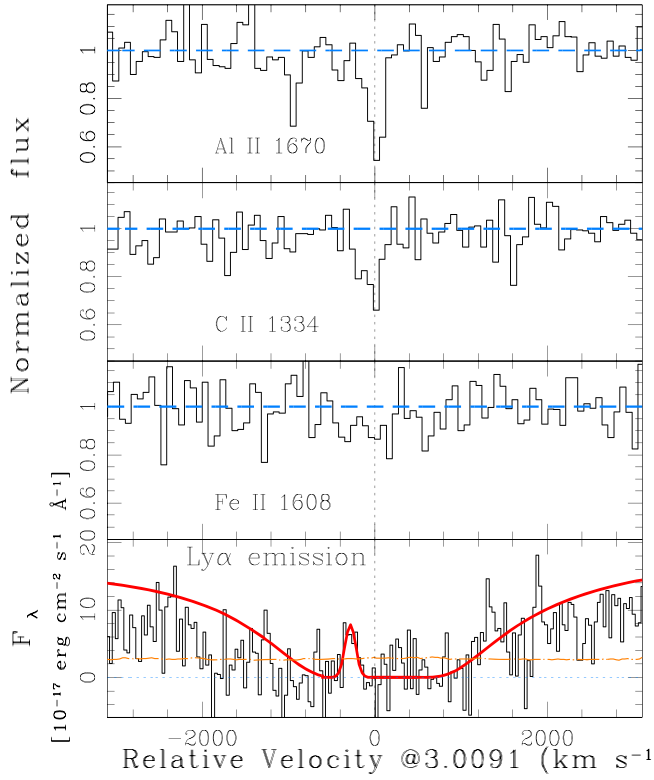

Figure 3. Velocity plots of absorption lines and the Lyα emission from DLA host galaxy. The zero velocity is defined with respect to the DLA redshift at $z_{\rm abs} = 3.0091 \pm 0.0001$. The bottom panel shows the Lyα emission extracted in an aperture radius of 2″ together with the best fitting Gaussian model. In the top panels, we plot absorption line profiles of Al II, C II, and Fe II detected in SDSS spectrum.

Focusing on the properties of the emission line next, a single component Gaussian fit to the Lyα line gives an intrinsic FWHM (i.e., deconvolved from instrumental effects) of $\approx$131 km s^{-1} and a velocity dispersion of $\sigma \approx 56$ km s^{-1}. The Lyα emission is found to be blueshifted from the systemic redshift of $z_{\rm abs} \approx 3.0091$ derived from metal absorption lines (see upper three panels of Figure 3) by 281 ± 43 km s^{-1}. The flux of the Lyα line is found to be $f_{\rm Ly\alpha} = (4.9 \pm 0.9) \times 10^{-17}$ erg s^{-1} cm^{-2} detected at 5.3σ level which reduces to 3.9σ level after accounting for the correlated noise (see Figure 2). This corresponds to a Lyα luminosity of $L_{\rm Ly\alpha} = (3.8 \pm 0.7) \times 10^{42}$ erg s^{-1} at the DLA redshift. Although the detection significance is marginal from a statistical point of view, the presence of an emission feature exactly at the expected location from the SDSS spectrum further strengthens the case for real detection.

In order to identify the location of the galaxy responsible for Lyα emission, we generate a Lyα emission map integrated over a velocity window from $v = -450$ km s^{-1} to $v = -187$ km s^{-1}, comprising the Lyα emission feature. The left panel of Figure 4 shows the Lyα emission map, revealing the location of the DLA host galaxy. Given the poor spatial resolution of PCWI, we could only place an upper limit on the extent of the Lyα emission to be $<$30 kpc, at a surface brightness limit of $\Sigma_{\rm Ly\alpha} > 10^{-17.5}$ erg s^{-1} cm^{-2} arcsec^{-2}. The right panel of Figure 4 shows instead the quasar image in the continuum after collapsing the cube. The overlayed contours mark the Lyα emission map at the flux levels of 0.20, 0.25, 0.30 $\times$ 10^{-17} erg s^{-1} cm^{-2}.

It is clear from the figure that the peak flux of the Lyα emission (marked as a cross symbol) is off-centered from the quasar (marked as a diamond). More quantitatively, we have calculated the separation between quasar and DLA host galaxy based on a light-weighted center, finding 0.″6 with a corresponding projected distance of 5 kpc. Given that the offset is less than the pixel scale we consider this as a lower limit. In addition, constrained by the pixel size we measure an upper limit on impact parameter of 12 kpc (see also, Figure 5).

5. Discussion and Conclusion

We report the detection of Lyα emission from the host galaxy of a DLA with $\log N$(H I)[cm^{-2}] $= 21.0 \pm 0.10$ at $z_{\rm abs} = 3.0091$ toward the background quasar SDSS J011852+040644 at $z_{\rm em} = 3.226$. The DLA host is detected, by selection, at a small impact parameter of $\lesssim$12 kpc with Lyα luminosity of $L_{\rm Ly\alpha} = (3.8 \pm 0.7) \times 10^{42}$ erg s^{-1}, which is typical of the characteristic luminosity ($\log L_\star$[erg s^{-1}] $= 42.66$) of the Lyα emitter galaxies at $z \sim 3$ (Herenz et al. 2019).

Given the resonant scattering nature of the Lyα line, the emergent profile is modified and suppressed by many physical effects, e.g., H I content, gas geometry and kinematics, and the dust content and distribution. For instance, in an optically thick static medium Lyα escapes through successive resonance scattering leading to a double-humped profile, with the position of the peaks determined by column density, temperature, and kinematics of the medium (Neufeld 1990; Dijkstra 2014). In addition, scattering through an inflowing (outflowing) medium leads to an overall blueshift (redshift) of the Lyα profile with enhanced blue (red) peak and suppressed red (blue) peak (Dijkstra et al. 2006, see below). In a pure static medium, the expected velocity offset of the Lyα emission is $\sim$344 km s^{-1} if we assume H I gas temperatures of 10^4 K (Dijkstra 2014, see their Equation (21)). For a column density of 10^{21} cm^{-2}, consistent with this DLA, a velocity of $\approx$300 km s^{-1} is expected, in line with our observations ($\approx$281 km s^{-1} with respect to the systemic redshift derived from metal absorption lines).

However, a static configuration is perhaps unlikely in real systems, and the blue offset seen for this DLA host may arise because of an inflowing gas geometry (e.g., Rauch et al. 2008, 2011). Dijkstra et al. (2006) have modeled the spectra and surface brightness distributions for the Lyα radiation from collapsing protogalaxies. They demonstrate that due to transfer of energy from the collapsing gas to the Lyα photons, together with a reduced escape probability for photons in their wing, the blue peak is significantly enhanced, which results in an effective blueshift of the Lyα line. Furthermore, employing a three-dimensional Lyα radiative transfer code, Laursen & Sommer-Larsen (2007) have investigated the properties of young Lyα emitting galaxies at high redshift ($z \sim 3$) from a cosmological galaxy formation simulation and found the dominant blue peak showing the signature of infalling gas (see also, Laursen et al. 2009). Such Lyα emission profiles with prominent blue peaks and suppressed red peaks, with typical offset of a few hundred km s^{-1} as seen here, have been observed in several Lyα blobs (Bower et al. 2004; Wilman et al. 2005), LAEs (Bunker et al. 2003) as well as one high-confidence DLA by Mackenzie et al. (2019) in VLT-MUSE observations.

Absorption lines from C II 1334 Å, Fe II 1608 Å, and Al II 1670 Å ions are detected in the SDSS spectrum with an equivalent width of 0.36 ± 0.04 Å, 0.25 ± 0.08 Å, and 0.59 ± 0.09 Å, respectively. Based on the strong correlation seen

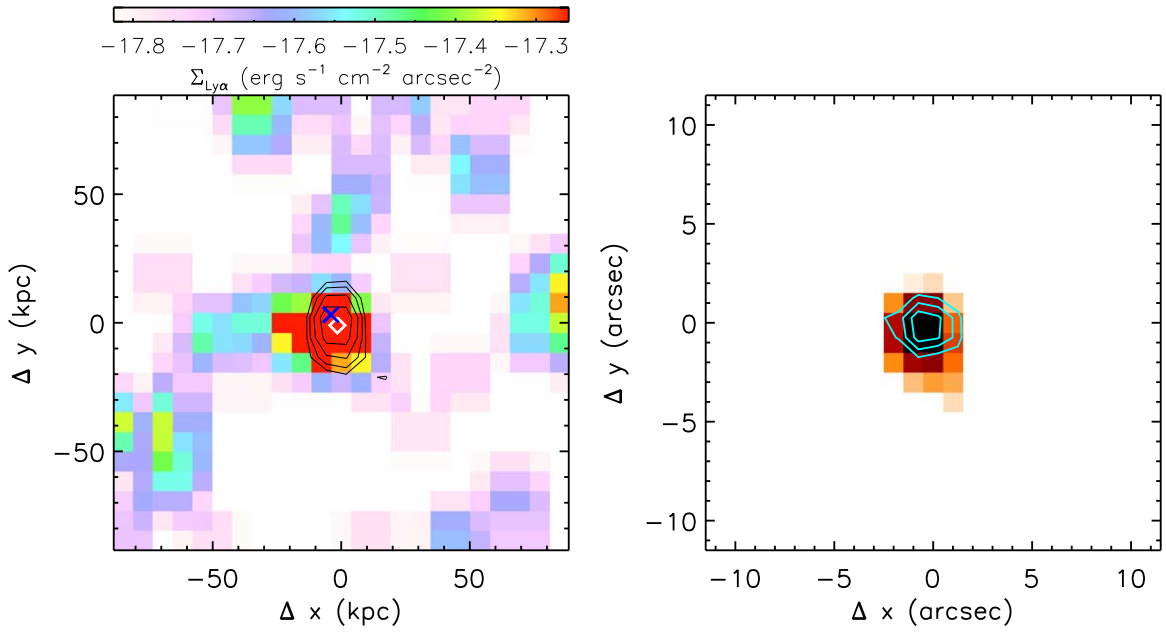

Figure 4. Left panel: the Lyα emission map integrated over a velocity window from $v = -450$ km s^{-1} to $v = -187$ km s^{-1}, comprising the Lyα emission feature, reveals the presence of DLA host galaxy at an impact parameter of $\lesssim$12 kpc. The black contours mark the continuum detected source (i.e., the quasar). The quasar and the DLA host galaxy centers are marked with a diamond and a cross, respectively. Right panel: the white-light image reconstructed from the PCWI data cube showing the quasar at the center. The cyan contours mark the Lyα emission map at the flux levels of 0.2, 0.25, 0.3 $\times$ 10^{-17} erg s^{-1} cm^{-2}.

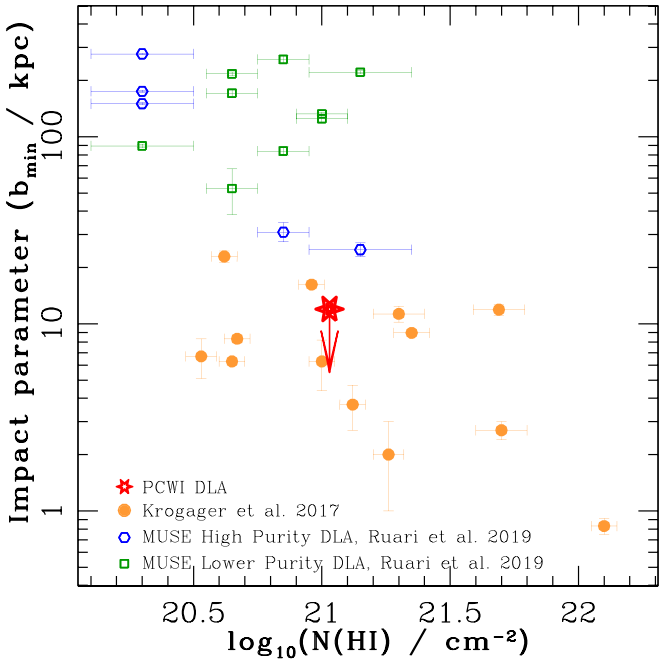

Figure 5. H I Column density vs. impact parameter relation for DLA host galaxies at $z > 1.5$. The filled circles show the DLAs identified over 25 yr in long-slit based spectroscopic searches, compiled by Krogager et al. (2017) as well as three extremely strong ($\log N$(H I)[cm^{-2}] $\geqslant$ 21.7) DLAs from Ranjan et al. (2020). The open diamonds show the galaxy population near DLAs from the recent MUSE survey by Mackenzie et al. (2019). The red star shows our PCWI DLA host galaxy detected at an impact parameter of $\lesssim$12 kpc.

between the rest-frame equivalent width of Si IIλ1526 line and metallicity, we derive an upper limit on the metallicity of $\log Z/Z_{\odot} < -1.58$ from the observed 3σ upper limit of 0.34 Å on Si IIλ1526 equivalent width (Prochaska et al. 2008; Jorgenson et al. 2013; Neeleman et al. 2013). In addition, we also derive a metallicity of $\simeq$−2.13 based on C IIλ1334 line using the apparent optical depth method. This limit also places the DLA just below the average metallicity of the population at this redshift (Rafelski et al. 2012), and well below the typical metallicity of DLAs chosen for targeted searches toward enriched systems, which typically select DLAs with $\log Z/Z_{\odot} > -1.0$ (see, Krogager et al. 2017). To date, only one other DLA host at this low metallicity, namely J2358+0149 with $\log Z/Z\odot \simeq -1.7$ derived based on Si II absorption, is detected at small impact parameter of <15 kpc (Srianand et al. 2016).

Besides the detection of emission coincident with the DLA position, our PCWI search has allowed us to trace the environment of this DLA out to 80 kpc. However, apart from the detection of a fairly bright DLA host, no other galaxies are seen in the field, to a luminosity limit of 5.3×10^{41} erg s^{-1}. This is a somewhat rare occurrence compared to previous studies that have examined the large-scale environment of DLAs. For instance, efforts to directly image the DLA host galaxies show a very small probability of DLAs being associated with bright Lyman break galaxies at distances < 10–20 kpc. These studies favor instead associations with either faint, possibly isolated, star-forming galaxies or dwarf galaxies which are clustered with more massive LBGs (see, Fumagalli et al. 2015). Moreover, in a recent MUSE survey of 6 high redshift ($z > 3$) quasar sightlines with H I column density ranging between $20.3 \leqslant \log N$(H I)[cm^{-2}] $\leqslant 21.15$ Mackenzie et al. (2019) have traced the environment of DLA host galaxies out to 250 kpc, detecting five high-confidence Lyα emitting galaxies associated with three DLAs and nine lower-significance Lyα emission objects in five sightlines. The MUSE detections are typically found at relatively large impact parameters of >50 kpc, implying that DLAs generally trace the neutral gas in a wide variety of rich environments, including overdense structures with multiple members.

In Figure 5, we explore in more detail the known anticorrelation between the impact parameters versus N(H I). Considering only the high-confidence DLA associations from

the literature and the IFU-based searches probing large-scale environments, a clear trend seems to emerge, although with large scatter. Indeed, high N(H I) systems are observed at preferentially small impact parameters, with a Pearson's correlation coefficient of -0.544 and a p value of 0.029 (Zwaan et al. 2005; Péroux et al. 2011; Rubin et al. 2015; Krogager et al. 2017). It should however be noted that some of these detections rely on long-slit spectroscopic measurements, for which only small impact parameters are accessible. Larger samples studied with large format IFUs are needed to confirm the significance of this relation.

As a final point, we infer a value for the in situ star formation rate (SFR, ($\dot{M}_{\rm SF}$)) of this DLA host, by assuming that the Lyα photons mainly originate from H II regions around massive stars embedded in the DLAs. Assuming case-B recombination (Osterbrock & Ferland 2006),

$$L_{\rm Ly\alpha} = 0.68 h\nu_{\alpha}(1 - f_{\rm esc}) N_{\gamma} \dot{M}_{\rm SF}, \quad (1)$$

where $h\nu_{\alpha} = 10.2$ eV [erg s^{-1}] is the energy of the Lyα photons, $f_{\rm esc}$ is the fraction of ionizing photons that escape before giving rise to ionization, and N_{γ} represents the number of ionizing photons released per baryon of star formation.

At the redshift of interest of this work, the escape fraction of Lyman continuum photons is found to vary over a range of $0 \lesssim f_{\rm esc} \lesssim 0.29$ with an average value of $f_{\rm esc} \sim 0.09$, as inferred by the Keck Lyman Continuum Spectroscopic Survey of star-forming galaxies at $z \sim 3$ (Steidel et al. 2018). We further assume $N_{\gamma} = 9870$, corresponding to the average metallicity, i.e., $\log Z/Z_{\odot} = -1.5$, of high redshift DLA absorbers and a Salpeter initial mass function with $\alpha = 2.35$, as given in Rahmani et al. (2010, and references therein). The observed Lyα luminosity also depends on the escape fraction ($f_{\rm esc}^{\rm Ly\alpha}$) of Ly$\alpha$ photons, and it is related to the emitted Lyα luminosity ($L_{\rm Ly\alpha}$) as $L_{\rm Ly\alpha}^{\rm obs} = f_{\rm esc}^{\rm Ly\alpha} L_{\rm Ly\alpha}$. The Ly$\alpha$ escape fraction increases smoothly and monotonically out to $z \sim 6$ and strongly depends on the dust content (Hayes et al. 2011). At the redshift of our interest the $f_{\rm esc}^{\rm Ly\alpha} \approx 5\% \pm 3\%$, as is estimated for the high-redshift ($z \sim 3$) star-forming galaxies by Hayes et al. (2010, 2011, see their Table 1).

Following this method, we infer that the DLA host galaxy is forming stars at $\dot{M}_{\rm SF} \approx 21 M_{\odot}$ yr^{-1} for an average $f_{\rm esc} \approx 9\%$ and $f_{\rm esc}^{\rm Ly\alpha} \approx 5\%$. However, this value is highly uncertain and ranges between $2 \leqslant \dot{M}_{\rm SF} \leqslant 53$ [$M_{\odot}$ yr^{-1}] if we account for the large uncertainty in the Lyα escape fraction from 70% to 2%, respectively (see also, Kimm et al. 2019). A similar SFR of $\sim 2 M_{\odot}$ yr^{-1} is also inferred from the star formation rate calibration for Hα luminosity [i.e., $L_{\rm H\alpha}$[erg s^{-1}] $= 10^{41.27} *$ SFR $M_{\odot}$ yr^{-1}] from Kennicutt & Evans (2012) and the intrinsic Lyα/Hα ratio of 8–10. This is comparable with the typical SFR of Lyman break galaxies at the similar redshifts (Kornei et al. 2010).

In conclusion, our search for DLA hosts of high column density ($\log N$ (H I) $\geqslant 21$) systems, with no metallicity preselection but identified on the basis of likely presence of Lyα emission in the SDSS fiber, appears to be effective in uncovering the gas–galaxy connection in an interesting region of parameter space, where we expect a direct link between gas in absorption and star formation in emission (Rafelski et al. 2012, 2016). Therefore, future IFU observations (e.g., PCWI, MUSE, KCWI) of our sample are likely to yield additional bright DLA host galaxies at small impact parameters, with which we can start to investigate more systematically both the galaxy population on large scales, and how neutral gas relates directly to star formation on smaller scales.

We thank the anonymous referee for useful comments. This research uses data obtained through the Telescope Access Program (TAP). This work was supported by the National Key R&D Program of China (2016YFA0400702, 2016YFA0400703), the National Science Foundation of China (11473002, 11721303, 11533001) and China Postdoctoral Science Foundation Grants (2018M630024, 2019T120011). M.F. acknowledges support by the Science and Technology Facilities Council [grant No. ST/P000541/1]. This project has received funding from the European Research Council (ERC) under the European Union's Horizon 2020 research and innovation program (grant agreement No. 757535). This project has received funding from the European Research Council (ERC) under the European Union's Horizon 2020 research and innovation program (grant agreement No. 757535). This work has been supported by Fondazione Cariplo, grant No. 2018-2329. P.N. acknowledges support from the French *Agence Nationale de la Recherche* under grant No. ANR-17-CE31-0011-01. Observations obtained with the Hale Telescope at Palomar Observatory were obtained as part of an agreement between the National Astronomical Observatories, Chinese Academy of Sciences, and the California Institute of Technology. Funding for the Sloan Digital Sky Survey IV has been provided by the Alfred P. Sloan Foundation, the U.S. Department of Energy Office of Science, and the Participating Institutions. SDSS-IV acknowledges support and resources from the Center for High-Performance Computing at the University of Utah. The SDSS website is www.sdss.org. SDSS-IV is managed by the Astrophysical Research Consortium for the Participating Institutions of the SDSS Collaboration including the Brazilian Participation Group, the Carnegie Institution for Science, Carnegie Mellon University, the Chilean Participation Group, the French Participation Group, Harvard-Smithsonian Center for Astrophysics, Instituto de Astrofísica de Canarias, The Johns Hopkins University, Kavli Institute for the Physics and Mathematics of the Universe (IPMU)/University of Tokyo, Lawrence Berkeley National Laboratory, Leibniz Institut für Astrophysik Potsdam (AIP), Max-Planck-Institut für Astronomie (MPIA Heidelberg), Max-Planck-Institut für Astrophysik (MPA Garching), Max-Planck-Institut für Extraterrestrische Physik (MPE), National Astronomical Observatories of China, New Mexico State University, New York University, University of Notre Dame, Observatário Nacional/MCTI, The Ohio State University, Pennsylvania State University, Shanghai Astronomical Observatory, United Kingdom Participation Group, Universidad Nacional Autónoma de México, University of Arizona, University of Colorado Boulder, University of Oxford, University of Portsmouth, University of Utah, University of Virginia, University of Washington, University of Wisconsin, Vanderbilt University, and Yale University.

ORCID iDs

Ravi Joshi https://orcid.org/0000-0002-5535-4186
Michele Fumagalli https://orcid.org/0000-0001-6676-3842
Raghunathan Srianand https://orcid.org/0000-0002-9062-1921
Pasquier Noterdaeme https://orcid.org/0000-0002-5777-1629
Marc Rafelski https://orcid.org/0000-0002-9946-4731
Qiong Li https://orcid.org/0000-0002-3119-9003
Zheng Cai https://orcid.org/0000-0001-8467-6478
Siwei Zou https://orcid.org/0000-0002-3983-6484
Xue-Bing Wu https://orcid.org/0000-0002-7350-6913

Linhua Jiang https://orcid.org/0000-0003-4176-6486
Luis C. Ho https://orcid.org/0000-0001-6947-5846

References

Altay, G., & Theuns, T. 2013, MNRAS, 434, 748
Bigiel, F., Leroy, A., Walter, F., et al. 2008, AJ, 136, 2846
Bower, R. G., Morris, S. L., Bacon, R., et al. 2004, MNRAS, 351, 63
Bunker, A. J., Stanway, E. R., Ellis, R. S., McMahon, R. G., & McCarthy, P. J. 2003, MNRAS, 342, L47
Christensen, L., Møller, P., Fynbo, J. P. U., & Zafar, T. 2014, MNRAS, 445, 225
Christensen, L., Noterdaeme, P., Petitjean, P., Ledoux, C., & Fynbo, J. P. U. 2009, A&A, 505, 1007
Cortese, L., Catinella, B., Boissier, S., Boselli, A., & Heinis, S. 2011, MNRAS, 415, 1797
Dijkstra, M. 2014, PASA, 31, 40
Dijkstra, M., Haiman, Z., & Spaans, M. 2006, ApJ, 649, 14
Fumagalli, M., Mackenzie, R., Trayford, J., et al. 2017, MNRAS, 471, 3686
Fumagalli, M., O'Meara, J. M., Prochaska, J. X., Kanekar, N., & Wolfe, A. M. 2014, MNRAS, 444, 1282
Fumagalli, M., O'Meara, J. M., Prochaska, J. X., Rafelski, M., & Kanekar, N. 2015, MNRAS, 446, 3178
Fynbo, J. P. U., Heintz, K. E., Neeleman, M., et al. 2018, MNRAS, 479, 2126
Fynbo, J. P. U., Laursen, P., Ledoux, C., et al. 2010, MNRAS, 408, 2128
Fynbo, J. P. U., Ledoux, C., Noterdaeme, P., et al. 2011, MNRAS, 413, 2481
Gawiser, E., van Dokkum, P. G., Herrera, D., et al. 2006, ApJS, 162, 1
Genzel, R., Tacconi, L. J., Gracia-Carpio, J., et al. 2010, MNRAS, 407, 2091
Harris, D. W., Jensen, T. W., Suzuki, N., et al. 2016, AJ, 151, 155
Hayes, M., Östlin, G., Schaerer, D., et al. 2010, Natur, 464, 562
Hayes, M., Schaerer, D., Östlin, G., et al. 2011, ApJ, 730, 8
Herenz, E. C., Wisotzki, L., Saust, R., et al. 2019, A&A, 621, A107
Janowiecki, S., Catinella, B., Cortese, L., et al. 2017, MNRAS, 466, 4795
Jorgenson, R. A., Murphy, M. T., & Thompson, R. 2013, MNRAS, 435, 482
Joshi, R., Srianand, R., Noterdaeme, P., & Petitjean, P. 2017, MNRAS, 465, 701
Kanekar, N., Sethi, S., & Dwarakanath, K. S. 2016, ApJL, 818, L28
Kennicutt, R. C., & Evans, N. J. 2012, ARA&A, 50, 531
Kimm, T., Blaizot, J., Garel, T., et al. 2019, MNRAS, 486, 2215
Klitsch, A., Zwaan, M. A., Péroux, C., et al. 2019, MNRAS, 482, L65
Kornei, K. A., Shapley, A. E., Erb, D. K., et al. 2010, ApJ, 711, 693
Krogager, J.-K., Fynbo, J. P. U., Møller, P., et al. 2012, MNRAS, 424, L1
Krogager, J. K., Møller, P., Fynbo, J. P. U., & Noterdaeme, P. 2017, MNRAS, 469, 2959
Kulkarni, V. P., Hill, J. M., Schneider, G., et al. 2000, ApJ, 536, 36
Laursen, P., & Sommer-Larsen, J. 2007, ApJL, 657, L69
Laursen, P., Sommer-Larsen, J., & Andersen, A. C. 2009, ApJ, 704, 1640
Ledoux, C., Petitjean, P., Fynbo, J. P. U., Møller, P., & Srianand, R. 2006, A&A, 457, 71
Mackenzie, R., Fumagalli, M., Theuns, T., et al. 2019, MNRAS, 487, 5070
Martin, D. C., Chang, D., Matuszewski, M., et al. 2014, ApJ, 786, 106
Möller, P., Fynbo, J. P. U., & Fall, S. M. 2004, A&A, 422, L33
Møller, P., Fynbo, J. P. U., Ledoux, C., & Nilsson, K. K. 2013, MNRAS, 430, 2680
Neeleman, M., Kanekar, N., Prochaska, J. X., et al. 2018, ApJL, 856, L12
Neeleman, M., Prochaska, J. X., Zwaan, M. A., et al. 2016, ApJL, 820, L39
Neeleman, M., Wolfe, A. M., Prochaska, J. X., & Rafelski, M. 2013, ApJ, 769, 54
Neufeld, D. A. 1990, ApJ, 350, 216
Noterdaeme, P., Petitjean, P., Carithers, W. C., et al. 2012, A&A, 547, L1
Noterdaeme, P., Petitjean, P., Ledoux, C., & Srianand, R. 2009, A&A, 505, 1087
Noterdaeme, P., Petitjean, P., Pâris, I., et al. 2014, A&A, 566, A24
Osterbrock, D. E., & Ferland, G. J (ed.) 2006, Astrophysics of Gaseous Nebulae and Active Galactic Nuclei (Mill Valley, CA: Univ. Science Books)
Péroux, C., Bouché, N., Kulkarni, V. P., York, D. G., & Vladilo, G. 2011, MNRAS, 410, 2251
Péroux, C., Bouché, N., Kulkarni, V. P., York, D. G., & Vladilo, G. 2012, MNRAS, 419, 3060
Péroux, C., McMahon, R. G., Storrie-Lombardi, L. J., & Irwin, M. J. 2003, MNRAS, 346, 1103
Prochaska, J. X., Chen, H.-W., Wolfe, A. M., Dessauges-Zavadsky, M., & Bloom, J. S. 2008, ApJ, 672, 59
Prochaska, J. X., & Wolfe, A. M. 2009, ApJ, 696, 1543
Rafelski, M., Gardner, J. P., Fumagalli, M., et al. 2016, ApJ, 825, 87
Rafelski, M., Neeleman, M., Fumagalli, M., Wolfe, A. M., & Prochaska, J. X. 2014, ApJL, 782, L29
Rafelski, M., Wolfe, A. M., Prochaska, J. X., Neeleman, M., & Mendez, A. J. 2012, ApJ, 755, 89
Rahmani, H., Srianand, R., Noterdaeme, P., & Petitjean, P. 2010, MNRAS, 409, L59
Ranjan, A., Noterdaeme, P., Krogager, J. K., et al. 2020, A&A, 633, A125
Rauch, M., Becker, G. D., Haehnelt, M. G., et al. 2011, MNRAS, 418, 1115
Rauch, M., Haehnelt, M., Bunker, A., et al. 2008, ApJ, 681, 856
Rubin, K. H. R., Hennawi, J. F., Prochaska, J. X., et al. 2015, ApJ, 808, 38
Srianand, R., Hussain, T., Noterdaeme, P., et al. 2016, MNRAS, 460, 634
Steidel, C. C., Bogosavljević, M., Shapley, A. E., et al. 2018, ApJ, 869, 123
Tremonti, C. A., Heckman, T. M., Kauffmann, G., et al. 2004, ApJ, 613, 898
Wilman, R. J., Gerssen, J., Bower, R. G., et al. 2005, Natur, 436, 227
Wolfe, A. M., Gawiser, E., & Prochaska, J. X. 2005, ARA&A, 43, 861
Zwaan, M. A., van der Hulst, J. M., Briggs, F. H., Verheijen, M. A. W., & Ryan-Weber, E. V. 2005, MNRAS, 364, 1467